Clays and Clay Minerals, Vol. 48, No. 2, 238–246, 2000.

LOW-TEMPERATURE ACID WEATHERING IN NEWHAVEN, SUSSEX, UNITED KINGDOM, AND ITS APPLICATION TO THEORETICAL MODELING IN RADIOACTIVE WASTE-DISPOSAL SITES

THIERRY DE PUTTER,[1] ALAIN BERNARD,[2] ALAIN PERRUCHOT,[3] DOMINIQUE NICAISE[1], AND CHRISTIAN DUPUIS[1]

[1] Faculté Polytechnique de Mons, Géologie Fondamentale et Appliquée, 9 rue de Houdain, B-7000 Mons, Belgium
[2] Université Libre de Bruxelles, Géochimie et Minéralogie, CP 160/02, 50, av. F. Roosevelt, B-1050 Bruxelles, Belgium
[3] Université de Paris-Sud, Géochimie des Roches Sédimentaires, UMR-CNRS 8616, bâtiment 504, F-91405 Orsay cedex, France

Abstract—Tertiary weathered sediments located immediately to the west of the harbor at Newhaven, Sussex, UK, were investigated by examination of major and trace elements by scanning electron microscope (SEM), microprobe, and inductively coupled plasma mass spectrometer (ICP-MS), and the mineralogy was studied by optical petrography, X-ray diffraction (XRD), transmission electron microscope (TEM), selective leaching, and thermodynamic modeling. Studied outcrops experienced acid leaching by sulfuric acid percolating downward through Tertiary sediments overlying Cretaceous chalk. The progressive neutralization of the percolating acid fluids resulted in "sequentially" layered neoformation of minerals: jarosite, iron oxides, aluminous minerals (sulfates, oxyhydroxides), gypsum, and Fe-Mn oxides. Substantial agreement was found between field observations and mineral assemblages obtained by modeling with the program CHILLER. These results suggest that the initial assumptions on the weathering process and mechanisms are correct. The relevance and implications of this study in the modeling of future denudation and weathering processes of radioactive waste-disposal sites (both deeply buried sites for high-level waste and surface sites for low-level waste) are discussed. Neoformed phases, such as jarosite, aluminous minerals, and silico-aluminous gels may play a significant role in the efficient trapping of mobilized pollutant radionuclides.

Key Words—Acid Weathering, Aluminous Minerals, Jarosite, Radioactive-Waste Sites, Silico-Aluminous Gels, Thermodynamic Modeling.

INTRODUCTION

Thermodynamic modeling is of interest in its potential application to environmental remediation. One major "environmental" hazard where such modeling may be useful is the potential weathering of the argillaceous near-field (localized area around the gallery) of a deeply buried ("geological") high-level radioactive waste (HLW) site that undergoes future denudation and the clay cap of a surface-based site for low-level radioactive waste (LLW). We pay special attention to Belgian "reference" projects, where HLW may be sited in the Oligocene Boom Clay Formation (De Putter and Charlet, 1994) or LLW may be hosted in surface-based deposits with a clay cap (De Putter *et al.*, 1997).

Previously, we modeled the oxidation of pyrite contained in the Boom Clay Formation (~40 g/kg; Bernard *et al.*, 1997) and the buffering of the resulting sulfuric acid by the surrounding clay. Interestingly, the minerals with high surface area (iron oxides, kaolinite) form in all possible titration models. This occurs also in the Newhaven profile (this study), where jarosite, iron oxides, and silico-aluminous gels are formed. Such minerals with high surface area and/or amorphous phases play a significant role in the immobilization of radioactive pollutants. For example, the neoformation of U-rich nanometric Ce,Nd,La-containing monazite crystals was found to occur on neoformed kaolinite flakes in a Miocene cryptokarst from South Belgium (Nicaise *et al.*, 1996; De Putter *et al.*, unpubl.). Recently, Aja (1998) showed that distribution coefficients (log K_d) for Nd sorption onto kaolinite are similar to those computed for the same light rare-earth elements (LREE) onto oxides, such as vernadite (δMnO_2) and goethite [$\alpha FeO(OH)$], which generally have high capabilities for the sorption of cations. Neoformed coatings of U-rich yttrium phosphates and rare-earth elements (REE) phosphates were observed on iron oxides in Quaternary cryptodolines from the Mons Basin, South Belgium (De Putter *et al.*, 1999). Perruchot *et al.* (1992) showed that Si-rich gels are likely to extract selectively the "pollutant" cations of $(UO_2)^{2+}$ and $(NpO_2)^{2+}$ from aqueous solutions.

Our first objective in this work was to study the parageneses of neoformed minerals in a karstic depression in the Mesozoic chalk of southern England. The genesis of the vertically zoned mineral sequences was related to the decreasing acidity of the downward percolating weathering fluids. Our second objective was to determine if thermodynamic modeling (using the computer code CHILLER; Reed, 1982; Reed and Spycher, 1984; Spycher and Reed, 1989) can be applied to fluid-rock interactions in low-temperature acid-weathering systems. Previous successful applications were made to acid volcanic lakes and high-tem-

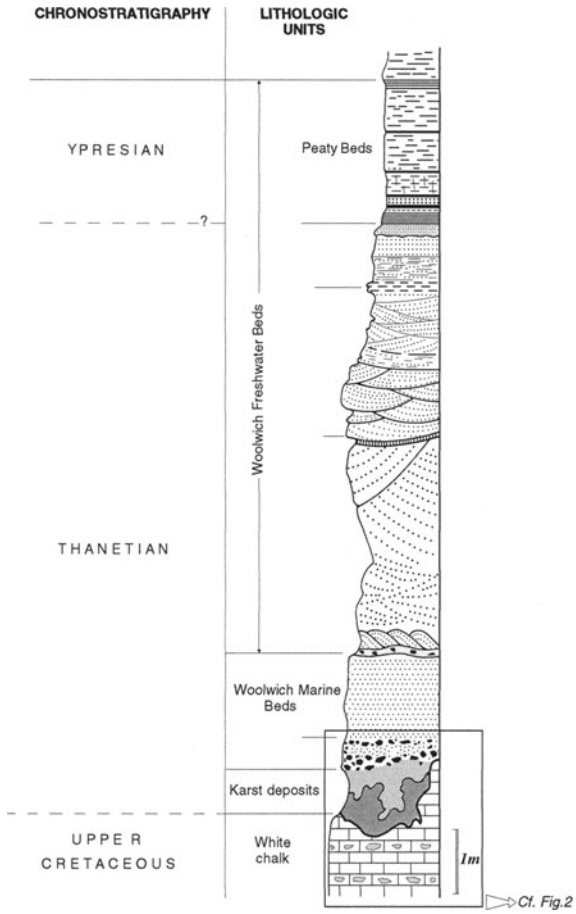

Figure 1. Lithologic column and chronostratigraphy of the Newhaven, Sussex beds. See enlargement of the box in the lower part of the lithologic column in Figure 2.

perature fumarolic environments (Delmelle and Bernard, 1994; Africano and Bernard, 2000).

GEOLOGICAL CONTEXT, PALYNOFACIES, AND MINERALOGY

Geology

Studied outcrops are located in the sea cliffs west of the west Pier of the harbor at Newhaven, Sussex, United Kingdom. These outcrops contain a few meters of Upper Cretaceous chalk, unconformably overlain by Upper Paleocene (Thanetian)/Lower Eocene (Ypresian) sediments, classically known as the "Woolwich Beds". The lower Woolwich Marine Beds (WMB) are glauconite-bearing marine sands. The upper part of the Woolwich Beds is freshwater (see Bone, 1976; Dupuis and Gruas-Cavagnetto, 1996). These Woolwich Freshwater Beds (WFB) are ~12 m thick and are grey/yellow cross-bedded fluviatile sands. The WFB are overlain by ~2 m of brown-grey silty/clayey sediments, known as Peaty Beds (PB). The Peaty Beds contain lignite layers, in which abundant vegetal remains and/or imprints of roots can be observed (Figure 1).

The studied sediments are located mostly within karstic depressions in the chalk, below the WMB (Figure 2). Previous studies of these weathering profiles documented the geology, palynology, and stratigraphy (Dupuis and Gruas-Cavagnetto, 1996) or focused on the aluminous minerals (aluminite, basaluminite, gibbsite, bayerite, and norstrandite) found in the karsts (Wilmot and Young, 1985). The karstic depressions that pre-date the Thanetian transgression (Dupuis and Gruas-Cavagnetto, 1996) most probably acted as "funnels" where the downward percolating fluids concentrated. Extensive mineral neoformation occurred in the depressions and in the voids created by karstification.

Palynofacies and mineralogy

The PB are the uppermost interval of the weathering profiles at Newhaven (Figure 1). Organic material of the PB is composed of black-brown carbonized remains of wood. This material is highly oxidized and corresponds to "degradofusinite" (M. Roche, pers. comm.). Root imprints and small vertical fissures are filled with jarosite [$KFe_3(SO_4)_2(OH)_6$] and gypsum ($CaSO_4{\cdot}2H_2O$), two common products of pyrite oxidation (see below).

The WFB are cross-bedded feldspathic fluviatile sands. They are extensively and homogeneously stained with neoformed bright-yellow jarosite. The upper WMB (~1 m) are glauconite-bearing sands that contain greenish flint pebbles. These pebbles are stained with orange iron oxides and yellow jarosite (samples NHN-1 to 4, Table 1; Unit 1, Figure 2). The lower WMB is comprised of ~0.5 m of greenish flint conglomerate, that locally reaches thicknesses to ~1 m and which fills the underlying karstic depressions (Unit 2, Figure 2).

Units 3 through 5 (Figure 2) infill karstic depressions. Silts bearing iron oxides vary considerably in thickness from a few centimeters to ~1 m, with a maximum thickness in karstic depressions (sample NHN-5, Table 1; Unit 3, Figure 2). A variable thickness of greenish-gray silt (sample NHN-13, Table 1; Unit 4, Figure 2) contains irregularly disseminated white nodules (samples NHN-7 to 11 and 14, Table 1). These nodules appear to be fibrous when dried. They consist of predominantly aluminous minerals and accessory iron oxides, halloysite, and micas (NHN-9).

ANALYTICAL METHODS AND RESULTS

The mineralogy of the sediments was determined by X-ray diffraction (XRD), using a diffractometer with a curved detector (INEL CPS 120) coupled with a multichannel analyzer. The mineral composition of the clay samples is obtained from oriented preparations of the <2-μm fraction by heat treatment at 110°C for 24 h and ethylene-glycol solvation. The formamide treat-

https://doi.org/10.1346/CCMN.2000.0480210 Published online by Cambridge University Press

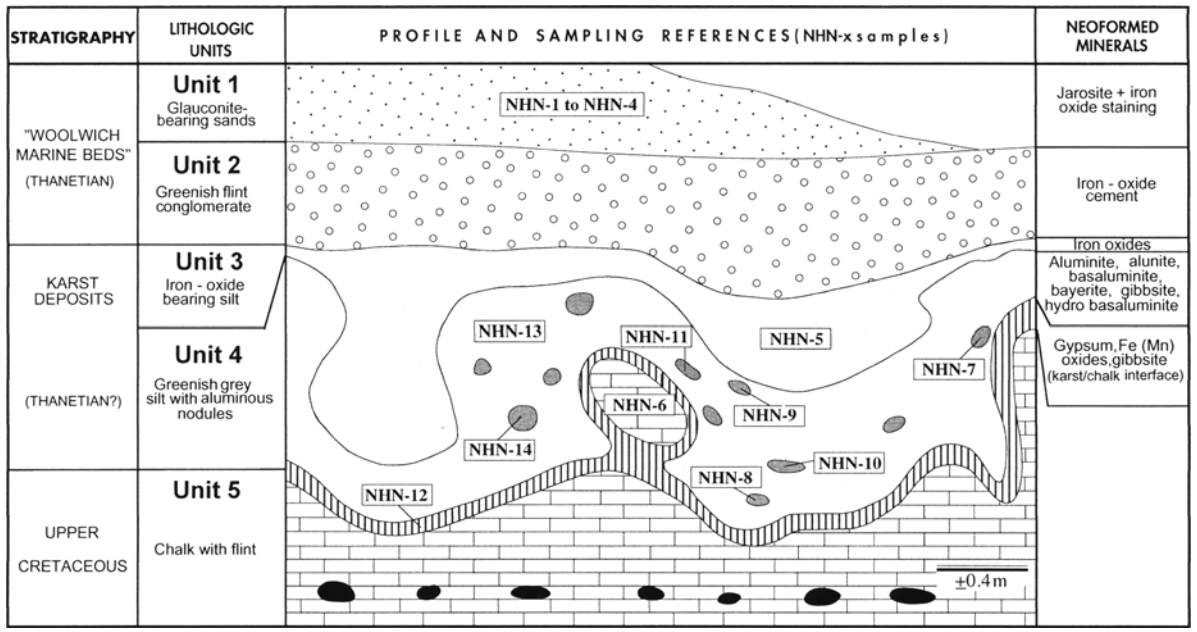

Figure 2. Sketch of the studied karstic deposits, with sample locations and neoformed mineralogy. Figure 2 is an enlargement of the lower part of Figure 1.

ment (Churchman *et al.,* 1984; Brouard, 1992), used to distinguish kaolinite and halloysite, and a semi-quantitative analysis were performed on randomly oriented preparations of samples dried at 110°C after grinding.

White nodules (NHN-7 to 11 and 14, Table 1) contain alunite [$KAl_3(SO_4)_2(OH)_6$], aluminite [$Al_2(SO_4)(OH)_4 \cdot 7H_2O$], basaluminite [$Al_4(SO_4)(OH)_{10} \cdot 5H_2O$], hydrobasaluminite [$Al_4(SO_4)(OH)_{10} \cdot 12–36H_2O$], gibbsite [$Al(OH)_3$], and bayerite [$Al(OH)_3$]. Selected XRD scans (samples NHN-7, 9, and 14) are shown in Figure 3. Norstrandite [$Al(OH)_3$] was reported by Wilmot and Young (1985), but was not found in the present work.

At and near the top of the irregularly weathered exposed chalk beds (sample NHN-6, Table 1; Unit 5, Figure 2), the silt/chalk interface consists of a centimeter-thick unit, comprised of gibbsite, gypsum, and Mn (+ accessory Co-Ni) oxides, with traces of barite (J. Jedwab, pers. comm.) (sample NHN-12, Table 1, Unit 5, Figure 2).

Transmission electron microscopy (TEM) studies were performed on a Jeol 100CX microscope. A drop of diluted suspension of the <2-μm clay fraction in distilled water was placed on a Cu grid and air-dried. Electron microprobe, scanning electron microscopy (SEM) and energy dispersive X-ray (EDX), infrared (IR), and inductively coupled plasma optical emission spectroscopy (ICP-OES) analysis were routinely performed to obtain additional chemical and mineralogical data (Tables 1 and 2).

We used selective leaching to evaluate the amorphous Si,Al-rich phase content of NHN-8, the Al-rich sample. Selective leaching occurs because Al- and Fe-bearing amorphous phases, as well as amorphous silico-aluminous phases ("gels"), are soluble in a Tamm oxalate buffer (0.2 M oxalate solution at pH = 3), whereas crystalline oxides are not. The Tamm procedure used here was modified by Schwertmann (1964); see also Bonneau and Souchier (1979).

The SiO_2/Al_2O_3 ratios of sample NHN-8 is 0.7 on the basis of powdered whole-rock analysis. The analysis suggests the presence of gibbsite and quartz (15.4 wt. % SiO_2; analytical procedure described above). The SiO_2/Al_2O_3 ratio of the Tamm leachate is 2.26 (Table 2), although allophane (gel) is typically characterized by $1 < SiO_2/Al_2O_3 < 2$ ratios (Wada 1979, 1982). Gel in sample NHN-8 is confirmed by TEM examination: abundant cloudy and/or spongy masses of poorly crystallized material are visible at low (30,000×) magnification in the TEM (Figure 4). Similar gels/allophanes were previously reported by Wilmot and Young (1985).

Chemical modeling involved the computer code CHILLER (Reed, 1982; Reed and Spycher, 1984; Spycher and Reed, 1989). The code uses a Newton-Raphson technique to solve sets of equations involving mass action and mass balance. These equations describe a gas-solid-aqueous system. The program performs reaction-path modeling, where the progress of the reaction is developed in a stepwise manner and complete heterogeneous equilibrium is computed at each step. CHILLER was used to model the generation of an acidic fluid resulting from the oxidation of pyrite. The program simulated the titration of this acidic

https://doi.org/10.1346/CCMN.2000.0480210 Published online by Cambridge University Press

Table 1. Detailed mineralogy based on XRD, IR, SEM, and microprobe data of samples NHN-1 to 14 (see location of the samples NHN-1 to 12 and NHN-14 in Figure 2).

Sample	Glauc.	Calc.	Qz	Gyps.	Bar.	Mica	Chl.	I–M	14–14	Sm	Kaol.	Hall.
NHN-1	X						0	67	6	27	Traces	
NHN-2	X						Traces	50	9	41	Traces	
NHN-3	X						0	32	9	58	1	
NHN-4	X						1	10	6	80	2	
NHN-6		X										
NHN-9						X						X
NHN-11			X									
NHN-12				X	traces							
NHN-13			X						X	X		X

	Goeth.	Hemat.	Jaros.	Mn ox.	Gibbs.	Bayer.	Alum.	Alumin.	B-alumin.	HB-alumn.
NHN-1	X		X							
NHN-2	X	X	X				?	?		
NHN-3	X	X	X							
NHN-4	X	X	X					?		
NHN-5	X									
NHN-7					X				X	X
NHN-8					X	X				
NHN-9	X				X		X			
NHN-10					X		X			
NHN-11					X					
NHN-12				X	X					
NHN-14								X		

Abbreviations: Glauc. = glauconite; Calc. = calcite; Qz = quartz; Gyps. = gypsum; Bar. = barite; Chl. = clorite; I-M = illite-mica; 14-14 = interstratified chlorite-smectite (vermiculite); Sm = smectite; Kaol. = kaolinite; Hall. = halloysite; Goeth. = goethite; Hemat. = hematite; Jaros. = jarosite; Mn ox. = manganese (and accessory Co-Ni) oxide; Gibbs. = gibbsite; Bayer. = bayerite; Alun. = alunite; Alumin. = aluminite; B-alumin. = basaluminite; HB-alumin. = hydrobasaluminite. Clay contents of samples NHN-1 to 4 are expressed in % of total clay. Note: X = presence; traces = minor quanities (<1%); ? = suspected presence, not confirmed.

fluid with glauconite-bearing WMB sand (below which is the karstic system studied here) and the chalk. Simulations were made at 1 atm total pressure with a step increment of 1 g of WMB sand added to 1 L of acid fluid. The chemical composition of unweathered glauconite-bearing WMB sands was required for the simulation. Unfortunately, there are no chemical data for these unweathered glauconite sands because unweathered outcrops do not exist. Thus, initial chemical data were estimated from comparable materials at different degrees of weathering from the study area and areas where similar strata occur.

Table 3 lists the chemical composition of the (apparently) less extensively weathered local sand (Newhaven "unweathered" sand, hereafter referred to as NH), a glauconite-bearing sand from South Belgium (Grandglise Formation), and the present mean chemical composition of weathered samples NHN-1 to 4 of the WMB sands. The Grandglise sand is less depleted in Al, Mg, Ca, and K (Table 3) than are the samples NH and NHN-x. We thus used the chemical composition of the Grandglise sand as an analogue for the "pre-weathering" chemistry of the local Newhaven sands. The validity of this assumption is consistent with the presence of jarosite in the simulation output (titration of 1 L of acid fluids by 410 g of glauconite-bearing sand and 20 g chalk, Figure 5). This suggests that the $[K^+]$ concentration of the glauconite-bearing Grandglise sand used as the starting composition in the model was sufficient to allow jarosite formation; when $[K^+]$ is too low, iron oxides compete successfully with jarosite.

Because the system is buffered with atmospheric oxygen, the Eh value was constrained by the O^{2-}/O_2 ratio. The initial Eh value was computed at 0.98 Volt (V) and was allowed to change during the titration (to 0.72 V by the end of the titration). All gases and solids produced in the system were allowed to fractionate as precipitates and/or gases. The equilibrium of dissolved SiO_2 was achieved with amorphous silica instead of chalcedony or quartz, by removing these polymorphs from the computation. This is justified because the formation of amorphous silica is favored in low-temperature acid environments and because significant quantities of Si are present in poorly crystallized phases as silico-aluminous gels or allophanes in Unit 4 (Figure 4). The use of chalcedony or quartz in the modeling only slightly decreases the level of silicic acid in solution because of the lower solubility of these polymorphs respective to amorphous silica (Fournier, 1985). Because no silicates are formed in the simulation, the use of chalcedony or quartz will increase the amount of solid silica present in the system at equilibrium.

https://doi.org/10.1346/CCMN.2000.0480210 Published online by Cambridge University Press

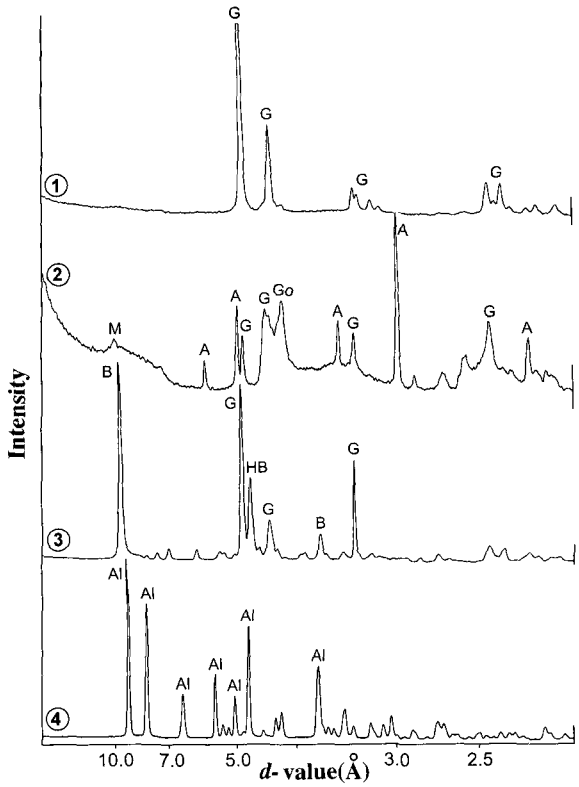

Figure 3. XRD scans (CoKα) of selected samples (1) NHN-12; (2) NHN-9; (3) NHN-7; (4) NHN-14. See location of the samples in Figure 2. Mineral abbreviations are as follows: A = alunite; Al = aluminite; B = basaluminite; G = gibbsite; Go = goethite; HB = hydrobasaluminite; M = mica. The peak at 7.2 Å on scan 2 (NHN-9) may be that of halloysite, but this is questionable.

WEATHERING PROCESS AND CHEMICAL MODELING

Neoformed Fe- and Al-rich minerals, including numerous sulfates [jarosite, alunite, aluminite, (hydro)basaluminite, gypsum] are present in the karst sediments. These phases suggest a weathering system involving the presence of sulfuric acid and other acid fluids to mobilize Fe and Al. Jarosite is an important indicator mineral of highly acidic conditions (pH values > ~2) in weathering profiles (Nordstrom, 1982; Van Breemen, 1982; Baron and Palmer, 1996; Herbert, 1997).

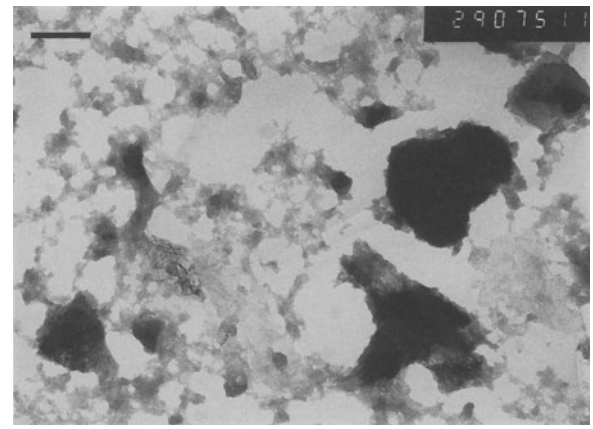

Figure 4. TEM micrograph of "cloudy" and/or "spongy" masses of poorly crystallized material, which are interpreted as silico-aluminous gels/allophanes. Sample NHN-8 (ultrasonically dispersed). Bar-scale is ~2500 Å.

Source of acidity in the system

Like Wilmot and Young (1985), we assume that acidity is a result of pyrite oxidation in the PB. Pyrite is not preserved in these beds, but organic material (black-brown carbonized wood) is highly oxidized, indicating that these beds underwent a strong oxidation episode. The overall reaction for complete pyrite oxidation and hydrolysis of iron to Fe(III) is: $FeS_2 + (15/4)O_2 + (7/2)H_2O \rightarrow Fe(OH)_3 + 2H_2SO_4$ (Nordstrom, 1982) which yields 2 moles of sulfuric acid per mole of pyrite. Fluids generated by this process are enriched in organic (humic, fulvic) and sulfuric acids. The contribution of organic acids to the increase in acidity was probably negligible. On the basis of computer modeling, the strongest acid of the mixture, sulfuric acid, lowers the pH of the fluids to ~1.2 (Figure 5).

Reaction of highly acidic fluids with sediments of the weathered profile

Initially, sulfuric acid released by the oxidation of pyrite is partially neutralized by silicate minerals from the surrounding sediments (PB, WFB, WMB). The related reaction (Delmelle and Bernard, 1994) is given as: $KAl_3Si_3O_{10}(OH)_2 + 10H^+ \rightarrow K^+ + Al^{3+} + 3H_4SiO_4$. The reaction consumes 10 moles of H^+ per mole of kaolinite and allows the pH to rise to a value where jarosite and other weathering minerals can form (see

Table 2. Chemical composition based on SEM-EDX analysis of NHN-8 nodule (dominant gibbsite and minor bayerite) and of NHN-8 residue, after TAMM leaching; chemical composition based on ICP-OES of NHN-8 TAMM leachate (sampling location in Figure 2). All values are expressed in wt. %.

Sample ref.	SiO_2	Al_2O_3	MgO	P_2O_5	SO_3	K_2O	CaO	Fe_2O_3	Total	SiO_2/Al_2O_3
NHN-8	24.71	59.84	0.00	3.06	5.12	0.19	1.22	5.86	100.00	0.70
NHN-8 residue	22.20	63.20	0.00	1.54	0.58	0.00	0.49	11.99	100.00	0.60
NHN-8 solution	—	—	—	—	—	—	—	—	—	2.26

https://doi.org/10.1346/CCMN.2000.0480210 Published online by Cambridge University Press

Table 3. Chemical composition based on SEM-EDX of two "candidate" sands for thermodynamic modeling ("NH 'unweathered' sand" and "Grandglise Fm" sand) and of samples NHN-1 to 4 (mean value; see sampling location in Figure 2). All values are expressed in wt. %.

Sample	SiO_2	Al_2O_3	Fe_2O_3	MnO	MgO	CaO	Na_2O	K_2O	TiO_2	P_2O_5	LOI	Total
NH 'unweathered' sand	87.00	2.85	4.33	0.00	0.55	0.12	0.12	1.35	0.21	0.02	3.45	100.00
Grandglise Fm (Belgium)	71.42	4.81	11.61	0.01	1.35	0.43	0.02	3.12	0.16	0.33	6.73	100.00
NHN-1 to 4 (mean value)	73.72	3.55	16.71	0.00	0.66	0.34	0.00	1.93	0.00	0.00	3.09	100.00

below). When the acid fluids generated in the PB are partially neutralized by silicates, pH increases and jarosite precipitates. The reaction for the formation of jarosite, as given by Baron and Palmer (1996), is: $K^+ + 3Fe^{3+} + 2SO_4^{2-} + 6H_2O \rightarrow KFe_3(SO_4)_2(OH)_6 + 6H^+$. Jarosite and iron oxides form in the upper part of the underlying WMB (Unit 1, Figure 2). The presence of iron oxides in the WMB (see Figure 5) suggests that neutralization of the acid fluids progresses downward, as iron oxides form in a more advanced stage of neutralization than jarosite (Nordstrom, 1982; Van Breemen, 1982). The hydrolysis of jarosite (Carson *et al.*, 1982) to ferric oxides, oxyhydroxides, or hydroxides is: $2KFe_3(SO_4)_2(OH)_6 + 6H_2O \rightarrow 6Fe(OH)_3 + K_2SO_4 + 3H_2SO_4$. Based on the simulations, jarosite now disappears (pH > ~1.5; see Figure 5) and iron oxides cement the flint conglomerate in the lower part of the WMB (Unit 2, Figure 2). These iron oxides, essentially goethite [αFeO(OH)] in the field, were represented by hematite (Fe_2O_3) in the simulation results (Figure 5), because the thermodynamic parameters for goethite are not available in the database. Iron oxides still formed in the first "true" karstic infilling layer encountered, *i.e.*, the silt layer of Unit 3 (Figure 2). Unit 4 (Figure 2) is, in the field, comprised of greenish-grey silt, which contains a wide variety of neoformed aluminum sulfates and/or hydroxides (alunite, aluminite, basaluminite, hydrobasaluminite, gibbsite; see above) disseminated in white lentils and nodules. Because alunite is the only Al-rich sulfate for which thermodynamic parameters are included in the database, it is the only Al-rich sulfate shown in the thermodynamic simulation (Figure 5). This sulfate, however, represents the entire range of Al-bearing minerals identified in the field. Thermodynamic calculations suggest that the pH was higher than ~2.3 at that stage (Figure 5).

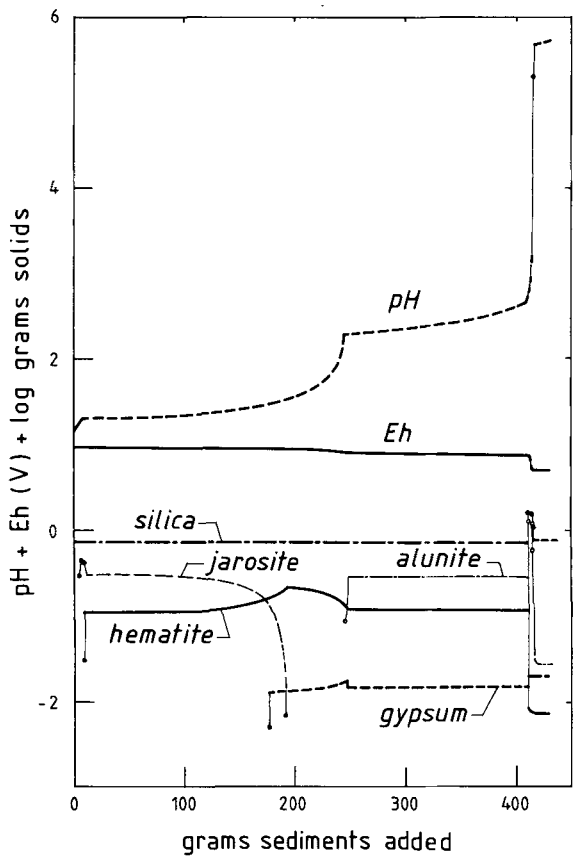

Figure 5. Thermodynamic model of the titration of acid fluids with 410 g of glauconite-bearing WMB sand (0–410 g on X-axis) and 20 g of chalk (>410 g on X-axis). Y-axis presents the quantity of neoformed solids (log grams solids), a pH scale (0–6, with no units), and an Eh scale (in Volts). The precipitation of solid phases (*i.e.*, hematite, alunite) is frequently associated with production of H^+ (*e.g.*, $K^+ + 3Fe^{3+} + 2SO_4^{2-} + 6H_2O \rightarrow KFe_3(SO_4)_2(OH)_6 + 6H^+$). Alunite temporarily counteracts the increase in pH owing to hydrolysis reactions (see text for further details).

The lower part of the decimeter-thick silts containing aluminous minerals is in contact with the chalk. We infer from the simulations that the chalk took a dominant role in the titration of the fluids, at least in the lowermost 10–15 cm of the silt unit, where the pH reached a value of ~2.7 (Figure 5). Simulations indicate that the titration of the residual acidity of the fluids involves a mere ~20 g of chalk/L of fluids.

The upper part of Unit 5 (Figure 2), at the karst infilling/chalk interface, is a decimeter-thick strip in which gypsum ($CaSO_4{\cdot}2H_2O$, where Ca^{2+} originates from chalk dissolution), gibbsite, and Mn-oxides (the latter mineral not shown in Figure 5) are mixed. Gypsum neoformation (Andrews *et al.*, 1996) is: $CaCO_3 + H_2SO_4 + H_2O \rightarrow CaSO_4{\cdot}2H_2O + CO_2$. This last stage was characterized by a steep increase in pH, from ~2.7 to ~5.75 (Figure 5). The concentration of alunite (representative of observed gibbsite) is lowered

https://doi.org/10.1346/CCMN.2000.0480210 Published online by Cambridge University Press

by a factor ~100 from pH ~ 5.7 onward. Concentrations of silica and hematite in the simulation, which may be representative of Mn oxides, are still lower. In the field as in the model, this step appears to be the final one in the titration of acid fluids. This step brings the pH to a high value (~5.75), close to that of meteoric waters in equilibrium with atmospheric CO_2 (Stumm and Morgan, 1996).

CONCLUSION

The present work documents the occurrence of sequentially layered mineral zones neoformed during the titration of downward-percolating acidic (pH ~ 1.2) fluids by glauconite-bearing sands and chalk. Neoformed minerals include, from top to bottom of the weathered profile: jarosite, iron oxides, Al-rich sulfates and hydroxides, gypsum, and Mn oxides. Many aluminous phases occur in the studied profile, including alunite, aluminite, basaluminite, hydrobasaluminite, gibbsite, and bayerite. The minerals are vertically zoned according to the decreasing acidity of the percolating fluids, from topmost jarosite (formed at pH < 1.5) to bottommost gypsum (formed at pH > 2.7). Aluminous minerals are formed at intermediate pH ranges (2.3 < pH < 3.3) and in the middle stratigraphic position in the field.

Substantial agreement was found between field observations and the mineral assemblages obtained by modeling. This agreement suggests the overall ability of the program CHILLER to model natural acid-weathering systems in low-temperature, sub-surface conditions. The main limitations in accuracy and predictability in the Newhaven profile are related to the lack of thermodynamic parameters for aluminous minerals, such as aluminite, basaluminite, hydrobasaluminite, and bayerite, and for manganese oxides.

Kargbo *et al.* (1993) emphasized the effects of sulfide-bearing clays (*i.e.,* pyrite-bearing clays) on the integrity of clay caps for landfills and surface impoundments: increasing the permeability of the cover to water, enhancing the erosion of the clay covers, and killing of vegetation. The authors however neglected to consider the positive effects of neoformed phases, such as jarosite, aluminous minerals, and silico-aluminous gels. For radioactive waste repositories, either deep-seated HLW sites undergoing denudation or a surface-based LLW site with a clay cap, we show that the neoformation of minerals with high surface areas and/or gels may allow for the efficient trapping of mobile trace elements during weathering (Perruchot *et al.,* 1992; Nicaise *et al.,* 1996; De Putter *et al.,* 1999; De Putter *et al.,* unpubl.).

Obviously, these results must be regarded cautiously, because the analogy between the studied natural systems and planned radioactive waste repositories is tenuous (for example, multiple man-made barriers in the repositories are not present or modeled in the natural system). Furthermore, chalk (as in the Newhaven karst) is not currently considered as a substrate for a waste repository. However, our results demonstrate that modeling of weathering of a radioactive waste repository in an argillaceous environment may be useful to predict the neoformation of minerals of high surface areas, which may play a significant role in the trapping of mobilized pollutant radionuclides.

ACKNOWLEDGMENTS

This research was funded by the Belgian Agency for the Management of Radioactive Waste (ONDRAF/NIRAS). M. Roche (Liège University, Belgium), J. Jedwab (Brussels University, Belgium), and P. Beaunier (Pierre et Marie Curie University, Paris, France) are thanked for their respective contribution on palynofacies determination, mineralogy, and TEM analyses. S. Guggenheim, M.E. Velbel, and two anonymous reviewers are thanked for providing helpful comments.

REFERENCES

Africano, F. and Bernard, A. (2000) Acid alteration in the fumarolic environment of Usu volcano, Hokkaido, Japan. *Journal of Volcanology and Geothermal Research,* in press.

Aja, S.U. (1998) The sorption of the rare earth element, Nd, onto kaolinite at 25°C. *Clays and Clay Minerals,* **46,** 103–109.

Andrews, J.E., Brimblecombe, P., Jickells, T.D., and Liss, P.S. (1996) *An Introduction to Environmental Chemistry.* Blackwell, Oxford, 209 pp.

Baron, D. and Palmer, C.D. (1996) Solubility of jarosite at 4–35°C. *Geochimica et Cosmochimica Acta,* **60,** 185–195.

Bernard, A., Jedwab, J., Van Moer, A., and Yourassowsky, N. (1997) *Rapport de Recherche: Le Piégeage de l'Iode Radioactif.* Internal Report, Department of Geochemistry and Mineralogy, Université Libre de Bruxelles, 63 pp.

Bone, D.A. (1976) The Tertiary deposits at Newhaven, Sussex. *Tertiary Research,* **1,** 47–49.

Bonneau, M. and Souchier, B. (1979). Constituants et propriétés du sol. In *Pédologie,* P. Duchaufour and B. Souchier, eds., Masson, Paris, 32–35.

Brouard, E. (1992) Etude des cryptokarsts tertiaires de la Forêt de la Bessède (Périgord, France) et de l'Entre-Sambre-et-Meuse (Belgique): Lithologie, géochimie, néogenèse et évolution des systèmes karstiques. Ph.D. thesis, Paris Sud-Orsay University, 270 pp.

Carson, C.D., Fanning, D.S., and Dixon, J.B. (1982) Alfisols and ultisols with acid sulfate weathering features in Texas. In *Acid Sulfate Weathering,* J.A. Kittrick, D.S. Fanning, and L.R. Hossner, eds., Soil Science Society of America Special Publication 10, Madison, Wisconsin, 127–146.

Churchman, G.J., Whitton, J.S., Claridge, G.G.C., and Theng, B.K.G. (1984) Intercalation method using formamide for differentiating halloysite from kaolinite. *Clays and Clay Minerals,* **32,** 241–248.

Delmelle, P. and Bernard, A. (1994) Geochemistry, mineralogy, and chemical modeling of the acid crater lake of Kawah Ijen Volcano, Indonesia. *Geochimica et Cosmochimica Acta,* **58,** 2445–2460.

De Putter, Th. and Charlet, J.-M. (1994) *Analogies Naturelles en Milieu Argileux.* ONDRAF (National Belgian Agency for Radioactive Waste Management) Report, NIROND 94-13, 183 pp.

De Putter, Th., André, L., Bernard, A., Charlet, J.-M., Dupuis, Ch., Jedwab, J., Nicaise, D., Perruchot, A., and Quinif, Y. (1997) *Analogies Naturelles et Archéologiques de Surface-*

Apports de la Géochimie de l'Altération et de l'Étude de la Durabilité des Matériaux à la Sûreté de l'Évacuation de Surface des Déchets Radioactifs de Faible Activité. ONDRAF (National Belgian Agency for Radioactive Waste Management) Report, NIROND 97-09, 141 pp.

De Putter, Th., Charlet, J.-M., and Quinif, Y. (1999) REE, Y and U concentration at the fluid-iron oxide interface in Late Cenozoic cryptodolines from Southern Belgium. *Chemical Geology,* **153,** 139–150.

Dupuis, C. and Gruas-Cavagnetto, C. (1996) The Woolwich Beds and the London Clay of Newhaven (East Sussex): New palynological and stratigraphical data *The London Naturalist,* **75,** 27–39.

Fournier, R.O. (1985) The behavior of silica in hydrothermal solutions. *Reviews in Economic Geology,* **2,** 45–60.

Herbert, R.B. (1997) Properties of goethite and jarosite precipitated from acidic groundwater, Dalarna, Sweden. *Clays and Clay Minerals,* **45,** 261–273.

Kargbo, D.M., Fanning, D.S., Inyang, H.I., and Duell R.W. (1993) Environmental significance of acid sulfate "clays" as waste covers. *Environmental Geology,* **22,** 218–226.

Nicaise, D., De Putter, Th., André, L., Jedwab, J., and Dupuis, C. (1996) Néoformation de phosphates nanométriques de terres rares en altération acide de basse température: Implications pour le piégeage des terres rares, de l'uranium et du thorium. *Comptes-Rendus de l'Académie des Sciences de Paris* (série IIa), **323,** 113–120.

Nordstrom, D.K. (1982) Aqueous pyrite oxidation and the consequent formation of secondary iron minerals. In *Acid Sulfate Weathering,* J.A. Kittrick, D.S. Fanning, and L.R. Hossner, eds., Soil Science Society of America Special Publication 10, Madison, Wisconsin, 37–55.

Perruchot, A., Delbove, F., Paulus, J.M., and Adloff, J.P. (1992) Behaviour of uranyl and neptunyl cations during ion exchange between silicate gels $pSiO_2$-(A,B)-nH_2O and aqueous solutions (A^{2+}, B^{2+}) (A^{2+} = UO_2^{2+}, NpO_2^{2+}; B^{2+} = Mg^{2+}, Ca^{2+}, Ni^{2+}): An experimental study. *Applied Geochemistry,* supplementary Issue, **1,** 95–107.

Reed, M.H. (1982) Calculation of multicomponent chemical equilibria and reaction processes in systems involving minerals, gases and an aqueous phase. *Geochimica et Cosmochimica Acta,* **46,** 513–528.

Reed, M.H. and Spycher, N. (1984) Calculation of pH and mineral equilibria in hydrothermal waters with application to geothermometry and studies of boiling and dilution. *Geochimica et Cosmochimica Acta,* **48,** 1479–1492.

Schwertmann U. (1964) Differenzierung der Eisenoxide des Bodens durch Extraktion mit Ammoniumoxalat Lösung. *Zeitschrift für Pflanzenernahrung und Bodenkunde,* **105,** 194–202.

Spycher, N. and Reed, M.H. (1989) CHILLER: A program for computing water-rock reactions, boiling, mixing and other reaction processes in aqueous-mineral-gas systems (revised preliminary edition). Department of Geological Sciences, University of Oregon, Eugene.

Stumm, W. and Morgan, J.J. (1996) *Aquatic Chemistry—Chemical Equilibria and Rates in Natural Waters.* Wiley, New York, 1022 pp.

Van Breemen, N. (1982) Genesis, morphology and classification of acid sulfate soils in coastal plains. In *Acid Sulfate Weathering,* J.A. Kittrick, D.S. Fanning, and L.R. Hossner, eds., Soil Science Society of America Special Publication 10, Madison, Wisconsin, 95–108.

Wada, K. (1979) Structural formulas of allophanes. In *Proceedings of the International Clay Conference (Oxford),* M.M. Mortland and V.C. Farmer, eds., Developments in Sedimentology 27, Elsevier, Amsterdam, 537–545.

Wada, K. (1982) Amorphous clay minerals—chemical composition, crystalline state, synthesis and surface properties. In *Proceedings of the International Clay Conference (Bologna),* H. van Olphen and F. Veniale, eds., Developments in Sedimentology 35, Elsevier, Amsterdam, 385–398.

Wilmot, R.D. and Young, B. (1985) Aluminite and other aluminium minerals from Newhaven, Sussex: The first occurrence of norstrandite in Great Britain. *Proceedings of the Geological Association,* **96,** 47–52.

E-mail of corresponding author: thierry.deputter@fpms.ac.be

(Received 18 March 1999; accepted 25 November 1999; Ms. 322; A.E. Michael A. Velbel)